University of Wollongong
Research Online

Faculty of Engineering and Information Sciences - Papers: Part B

Faculty of Engineering and Information Sciences

2018

A numerical simulation study on mechanical behaviour of coal with bedding planes under coupled static and dynamic load

Lihai Tan
University of Wollongong, Central South University, lt716@uowmail.edu.au

Ting X. Ren
University of Wollongong, tren@uow.edu.au

Xiaohan Yang
University of Wollongong, xy987@uowmail.edu.au

Xueqiu He
University of Wollongong, University of Science and Technology, hexq@uow.edu.au

Follow this and additional works at: https://ro.uow.edu.au/eispapers1

 Part of the Engineering Commons, and the Science and Technology Studies Commons

Recommended Citation

Tan, Lihai; Ren, Ting X.; Yang, Xiaohan; and He, Xueqiu, "A numerical simulation study on mechanical behaviour of coal with bedding planes under coupled static and dynamic load" (2018). *Faculty of Engineering and Information Sciences - Papers: Part B*. 1839.
https://ro.uow.edu.au/eispapers1/1839

Research Online is the open access institutional repository for the University of Wollongong. For further information contact the UOW Library: research-pubs@uow.edu.au

A numerical simulation study on mechanical behaviour of coal with bedding planes under coupled static and dynamic load

Abstract

To investigate the bedding influence on coal mechanical behaviour in underground environments such as coal or rock burst, simulations of dynamic SHPB tests of pre-stressed coal specimens with different bedding angles were carried out using a particle flow code 2-dimensional (PFC2D). Three impact velocities of 4, 8 and 12 m/s were selected to study dynamic behaviours of coal containing bedding planes under different dynamic loads. The simulation results showed that the existence of bedding planes leads to the degradation of the mechanical properties and their weakening effect significantly depends on the angle θ between the bedding planes and load direction. With θ increaseing from 0° to 90°, the strength first decreased and subsequently increased and specimens became most vulnerable when θ was 30° or 45°. Five failure modes were observed in the specimens in the context of macro-cracks. Furthermore, energy characteristics combined with ultimate failure patterns revealed that maximum accumulated energy and failure intensity have a positive relation with the strength of specimen. When bedding planes were parallel or perpendicular to loading direction, specimens absorbed more energy and experienced more violent failure with increased number of cracks. In contrast, bedding planes with θ of 30° or 45° reduced the specimens' ability of storing strain energy to the lowest with fewer cracks observed after failure.

Disciplines

Engineering | Science and Technology Studies

Publication Details

Tan, L., Ren, T., Yang, X. & He, X. (2018). A numerical simulation study on mechanical behaviour of coal with bedding planes under coupled static and dynamic load. International Journal of Mining Science and Technology, 28 (5), 791-797.

This journal article is available at Research Online: https://ro.uow.edu.au/eispapers1/1839

International Journal of Mining Science and Technology 28 (2018) 791–797

Contents lists available at ScienceDirect

International Journal of Mining Science and Technology

journal homepage: www.elsevier.com/locate/ijmst

A numerical simulation study on mechanical behaviour of coal with bedding planes under coupled static and dynamic load

Lihai Tan [a,b,*], Ting Ren [a], Xiaohan Yang [a], Xueqiu He [a,c]

[a] School of Civil, Mining and Environmental Engineering, University of Wollongong, NSW 2522, Australia
[b] School of Resources and Safety Engineering, Central South University, Changsha 410083, China
[c] School of Civil and Environmental Engineering, University of Science and Technology, Beijing 100083, China

ARTICLE INFO

Article history:
Received 11 June 2018
Received in revised form 21 July 2018
Accepted 5 August 2018
Available online 28 September 2018

Keywords:
Static–dynamic coupled loads
SHPB
Coal bedding angle
Strain energy
PFC2D

ABSTRACT

To investigate the bedding influence on coal mechanical behaviour in underground environments such as coal or rock burst, simulations of dynamic SHPB tests of pre-stressed coal specimens with different bedding angles were carried out using a particle flow code 2-dimensional (PFC2D). Three impact velocities of 4, 8 and 12 m/s were selected to study dynamic behaviours of coal containing bedding planes under different dynamic loads. The simulation results showed that the existence of bedding planes leads to the degradation of the mechanical properties and their weakening effect significantly depends on the angle θ between the bedding planes and load direction. With θ increaseing from 0° to 90°, the strength first decreased and subsequently increased and specimens became most vulnerable when θ was 30° or 45°. Five failure modes were observed in the specimens in the context of macro-cracks. Furthermore, energy characteristics combined with ultimate failure patterns revealed that maximum accumulated energy and failure intensity have a positive relation with the strength of specimen. When bedding planes were parallel or perpendicular to loading direction, specimens absorbed more energy and experienced more violent failure with increased number of cracks. In contrast, bedding planes with θ of 30° or 45° reduced the specimens' ability of storing strain energy to the lowest with fewer cracks observed after failure.
© 2018 Published by Elsevier B.V. on behalf of China University of Mining & Technology. This is an open access article under the CC BY-NC-ND license (http://creativecommons.org/licenses/by-nc-nd/4.0/).

1. Introduction

Rocks and coals underground at great depth are subjected to high static stress. When dynamic disturbances occur such as blasting, drilling and seismic event, the adjacent rock and coal experience both static and dynamic loads simultaneously. The physical behaviour of rock under coupled static–dynamic loads is quite different from that under only static or dynamic loads [1]. It is widely considered that during deep excavation, static stress, which results in static energy accumulation in the rock, is the intrinsic cause of rock failure or rock burst, while dynamic loads trigger off its occurrence as an external cause [2,3]. In other words, both static and dynamic loads contribute to rock failure especially rock burst underground.

The Split Hopkinson Pressure Bar (SHPB) system is one of the most common test systems that have been widely employed to study the dynamic mechanical properties and behaviour of coal and rock [4–8]. In addition, SHPB simulation using the DEM method has also been widely used for rock dynamic mechanical studies [9,10]. To study mechanical properties of rock specimens subjected to simultaneous coupled static and dynamic stress, Li and Zhou presented a new SHPB testing technique which takes axial static pre-stress into consideration, finding that the rock strength under coupled static and dynamic loads is generally higher than the dynamic strength under only impact loads [11]. Using this technique, Tao investigated the mechanical behaviour of rock specimens containing a circular hole and the results indicate that static and dynamic stress concentration around the hole causes primary failure and eventual macro failure in rock [12].

The above-mentioned studies mainly concentrated on intact specimens or those containing a circular hole. In practical engineering, however, the structure of rock and coal underground is always very complex with numerous defects. Natural tectonic coal is characterized by strong anisotropy caused by various complex joints and weak planes or cleats (Fig. 1). Though the overall mechanical behaviour of rock or coal with numerous pores and random joints can be presented by continuum models and empirical formulas, these models and formulas have difficulty in describing the influence of regular distributed defect sets within the rock mass [13].

When bedding planes, which can be widely found in rock and coal, are taken into consideration, the mechanical properties and

* Corresponding author at: School of Civil, Mining and Environmental Engineering, University of Wollongong, NSW 2522, Australia.
E-mail address: lt716@uowmail.edu.au (L. Tan).

https://doi.org/10.1016/j.ijmst.2018.08.009
2095-2686/© 2018 Published by Elsevier B.V. on behalf of China University of Mining & Technology.
This is an open access article under the CC BY-NC-ND license (http://creativecommons.org/licenses/by-nc-nd/4.0/).

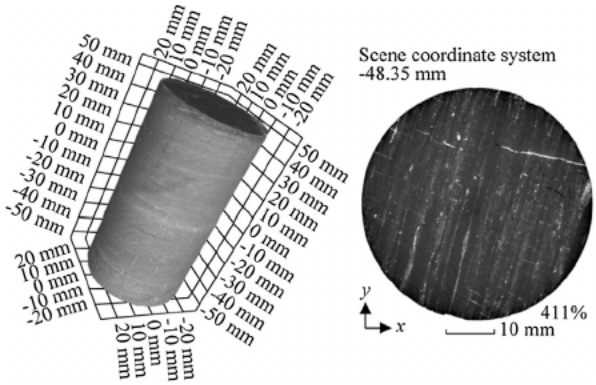

Fig. 1. Micro-scanning image of coal.

failure patterns in rock would be changed significantly [14–19]. Amadei developed analytical solutions to describe the strength of a regularly jointed rock mass and concluded that the strength of rock containing regular bedding planes are influenced by the interaction between intact part and bedding planes [20]. Based on dynamic Brazilian test, Zhao also suggested that both the failure pattern and dynamic tensile strength strongly depend on the bedding structure [21]. In his study, Liu showed the bedding effect, and concluded that the bedding effect on coal dynamic properties is less obvious than on static properties with strain rate increasing according to a series of quasi-static and dynamic uniaxial compression tests [22].

When it comes to rock burst or coal bump, energy characteristic is an important index to evaluate its propensity. During the compression process, the work is transformed into the elastic strain energy stored in rock, and dissipated energy in the form of surface energy, thermal energy, kinetic energy, etc. The history of deformation and failure in a rock sample is an integration of energy dissipation and energy release in the rock over time [23]. The capacity for storing and releasing strain energy and the environment for stress concentration and strain energy accumulation are the primary conditions for the occurrence of rock or coal burst in underground [24].

In practical engineering, the occurrence of coal burst is mostly caused by the superposition of dynamic loads and static loads. During the stress concentration and coal burst formation process, bedding planes will have important influence on the failure evolution and energy accumulation behaviour of coal. For underground coal mines, the dynamic loading such as mechanical impact, blasting loading and rock burst induced by high geo-stress could originate from any direction, and accordingly the coal failure could vary in different conditions. Therefore, further study about the influence of bedding angles on coal under dynamic loads is necessary for evaluation and prevention of coal bump or rock burst.

In this research, numerical models were developed and their micro-parameters calibrated against static compressive tests of intact specimen. Then, a series of pre-load SHPB numerical simulations were carried out to study the effect of the bedding angle on failure patterns, and the mechanical properties and strain energy of coal were investigated under coupled static-dynamic loads to improve the understanding of coal and rock burst induced by dynamic loads in underground mines.

2. Numerical models

In this research, numerical simulations were carried out using PFC2D, a discrete element method (DEM) soft. In PFC2D, rock materials are represented by bonded particles that interact at contacts by means of internal forces and moments. Contact mechanics is used to update internal forces and moments, and the movements of particles are computed according to Newton's laws of motion. Crack behaviour of rock can be modelled by allowing bonds at contact points to be broken when the inter-particle forces exceed either tensile or shear bond strength. In addition, the explicit solution scheme ensures that the numerical model can effectively simulate the crack propagation of rock materials and associated large displacements.

In the present simulation, a total of eight numerical specimens, numbered sequentially from S1 to S8 with dimensions of 50 mm × 50 mm (length × height) were established, as shown in Fig. 2. S1 is an intact numerical specimen without bedding. Parallel bedding planes are embedded in specimen S2 to S8. The bedding angel θ between bedding and loading direction from S2 to S8 are 0°, 15°, 30°, 45°, 60°, 75° and 90°, respectively. The vertical distance between two adjacent bedding planes is 10 mm.

The mechanical parameters in simulation were determined according to the laboratory compressive tests. The process to determine microscopic parameters is called calibration, a process in which a series of trial and error numerical simulations are performed to match laboratory-measured stress-strain curves. In this study, the standard compressive tests were conducted for calibration, and the obtained PFC microscopic parameters are listed in Table 1.

Stress-strain curves, failure patterns and mechanical properties of the coal specimen obtained from the laboratory experiment and the numerical simulation are presented in Fig. 3 and Table 2. The uniaxial compressive strength (UCS) and Young's modulus from the simulation are almost identical with their counterparts from the laboratory experiment with little deviation. Failure patterns in both cases are similar with shear failure dominating. The comparisons indicate that the microscopic parameters used in the numerical model are accurate and authentic. However, it should

Table 1
Microscopic parameters used in the PFC2D model.

Particle basic parameter		Parallel bond parameter	
Particle contact modulus E_c (GPa)	1.96	Elasticity modulus $\bar{E}_c$ (GPa)	1.96
Stiffness ratio k_n/k_s	4.1	Stiffness ratio k_n/k_s	4.1
Particle friction coefficient μ	0.577	Cohesion $\bar{c}$ (MPa)	16.5
Maximum particle radius R_{max} (mm)	0.2	Tensile strength $\bar{\sigma}_c$ (MPa)	10.0
Minimum particle radius R_{min} (mm)	0.3		
Particle density ρ (g/m^3)	1.4		

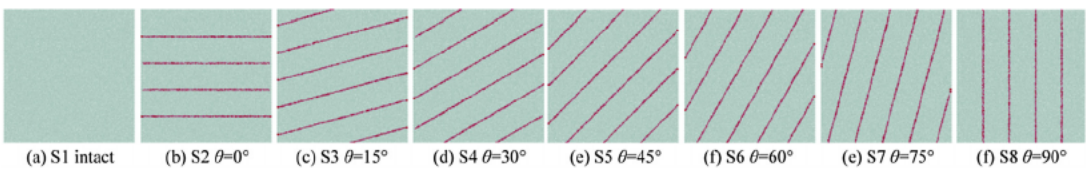

Fig. 2. Numerical specimen models: the red are bedding planes.

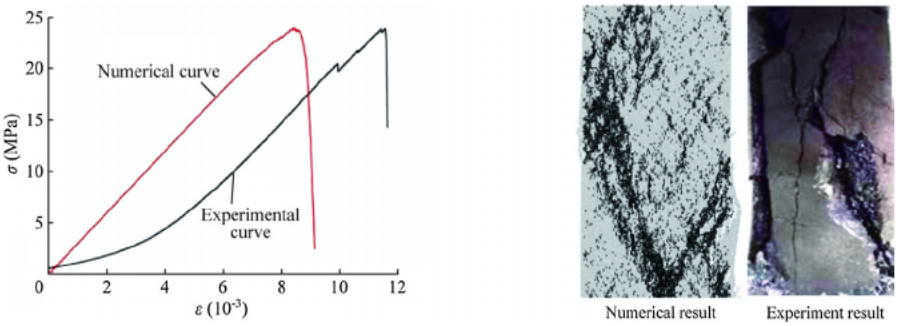

Fig. 3. Comparison between numerical and experiment results of intact specimen under uniaxial compression.

Table 2
Mechanical properties of intact specimen in laboratory experiment and PFC numerical simulation.

Mechanical property	Experimental result	Numerical result	Deviation
Peak stress (MPa)	23.86	23.92	0.25%
Young's modulus (GPa)	2.99	3.05	2.01%
Failure strain (10^{-3})	11.56	8.47	26.73%

be noticed that failure strain from experimental test is significantly greater than that from numerical simulation with a deviation of 26.73%. This is because there were numerous voids and pores in the coal specimen. The micro-image of the surface of a coal specimen, which was obtained using the scanning electron microscope (SEM), is given in Fig. 4. From Fig. 4, it can be observed that many pores with various shapes and sizes distribute in the coal. These pores resulted in a nonlinear deformation of the stress curve at early compression stage where those micro defects are gradually closed while this stage cannot be simulated by PFC2D [25,26].

The simulation model of the SHPB system was set up based on the coupled-load equipment developed by Li [11]. As shown in Fig. 5, the SHPB test system was established consisting of a striker, an incident bar, a transmitted bar, with a specimen sandwiched between them. The conical striker was suggested by International Society for Rock Mechanics (ISRM), which was necessary for producing half-sine waveform that contributes towards eliminating wave oscillation and reducing wave dispersion effects. The conical striker's advantage and reliability have been proved by many studies [27,28]. The end of the incident bar was restrained by a baffle screen and an axial pre-force was applied on the left end of the transmitted bar by pre-load unit to produce axial static pre-stress in the specimen. According to the rules established by ISRM, the lengths of incident bar and transmitted bar were selected to be 1.5 and 0.75 m, respectively. The diameter of the bars was 50 mm. In this study, the axial static pre-stress in specimens were set as 7.5 MPa, which caused linear elastic deformation in all cases before dynamic impact. The numerical model of the pre-load SHPB system is presented in Fig. 6.

According to the one-dimensional stress wave theory, stress (σ_s), strain (ε_s) and strain rate ($\dot{\varepsilon}_s$) of the specimen can be expressed as:

$$\sigma_S = \frac{A_B}{A_S} E_B \varepsilon_T \tag{1}$$

$$\varepsilon_s = -2\frac{C}{L_s} \int_0^t \varepsilon_R dt \tag{2}$$

$$\dot{\varepsilon}_s = -2\frac{C}{L_s} \varepsilon_R \tag{3}$$

where ε is the measured strain; the subscripts R and T the reflected and transmitted pulses, respectively; A_B and A_S the cross-section areas of the bar and specimen, respectively; and C the elastic wave speed in the bars.

The dynamic strength of a specimen determined by SHPB test is correct and valid only when stress in the specimen gets balanced before its instability, which needs the dynamic wave traveling through the specimen at least four times [29]. In Fig. 7, the typical stress waves in a SHPB test with an impact velocity of 8 m/s is presented. I, R, $I + R$ and T stand for the incident wave stress, reflected

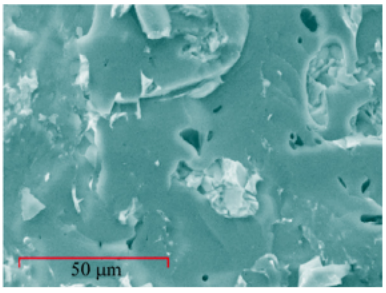

Fig. 4. SEM image of the coal specimen.

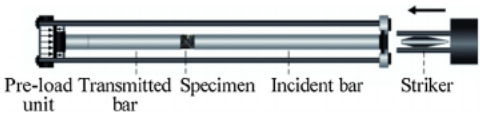

Fig. 5. Sketch of SHPB system with pre-load unit.

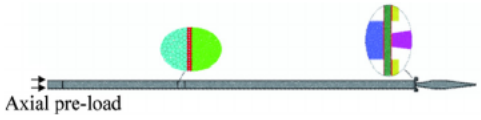

Fig. 6. Numerical model of SHPB test system.

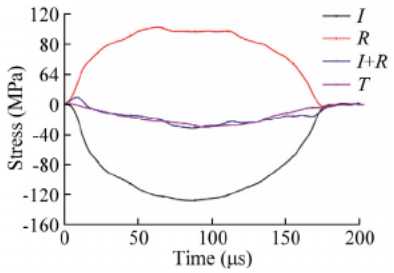

Fig. 7. Stress balance on the two ends of the specimen.

stress wave, the superposition of incident and reflected wave stress and the transmitted stress wave, respectively. It is obviously found that the stress waves at the incident end ($I + R$) and at the transmitted end (T) are in good agreement with each other, which manifests that the stress equilibrium in the specimen has been met well and highlights the validity and feasibility of SHPB simulation using PFC2D.

3. Numerical simulation of SHPB test

3.1. Failure mode

There exist three types of cracks for rock and coal in a 2D condition, namely tensile crack, shear crack and mixed crack, all of which can be identified based on the relative trend of displacement vectors along a macroscopic crack in PFC2D [30]. As similar failure characteristics were observed for the same specimen under different impact velocities, only the failure evolution of different specimens under an impact velocity of 8 m/s was presented as shown in Fig. 8. Timing started when the striker impacted the incident bar. For further determination of the failure mode, some typical cracks in Fig. 8 were analyzed using the displacement trend line method, which is shown in Fig. 9. In Fig. 8, black arrows show displacement vectors scaled by magnitude, blue arrows represent displacement trend directions, and blue dash lines denote macroscopic cracks. According to this method, cracks $A1$, $D1$, $E1$, $G2$ and $H2$ were determined as shear-dominated cracks, and crack $B1$, $D2$, $G1$ and $H1$ were considered as tensile-dominated cracks and the rest were mixed cracks.

Based on such determinations, failure evolution for these specimens was discussed. For the intact specimen, as shown in Fig. 8a, cracks first nucleated in the middle of the right side, and then the cracks formed into a rhombic failure zone and fractured the specimen. After that, the specimen was rapidly damaged by shear-dominated failure. For specimens containing bedding planes, cracks initially nucleated along bedding planes caused by their splitting or sliding. When $\theta = 0°$, the dominated failure was still characterized by shear cracks while bedding planes were split by tensile failure (Fig. 8b). For specimens containing inclined bedding planes with θ of 15°, the specimen was finally damaged by mixed tensile-shear failure along bedding planes and tensile-dominated cracks run through them (Fig. 8e). For specimens containing inclined bedding planes with θ from 30° to 45°, failure modes were still predominated by cracks through and along bedding planes (Figs. 8d and 7e). However, the bedding planes were mainly damaged by shear failure (crack $D1$ and $E1$ in Fig. 9). With θ increasing into the range from 60° to 75°, the failure of bedding planes was caused by mixed cracks again. Though there were cracks concentrating along bedding planes, overall specimen instability was caused by inclined shear failure more than bedding planes failure. When $\theta = 90°$, the instability of specimen was still mainly caused by shear failure while the bedding planes split by tensile failure (Fig. 8h).

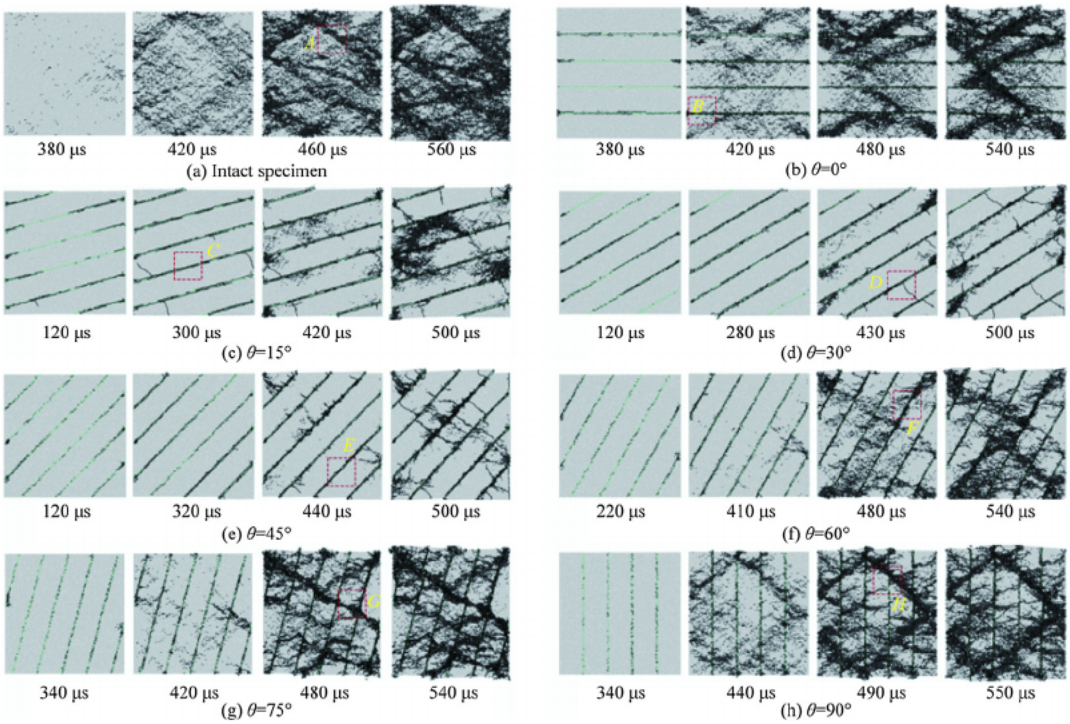

Fig. 8. Failure evolution of different specimens under impact velocity of 8 m/s.

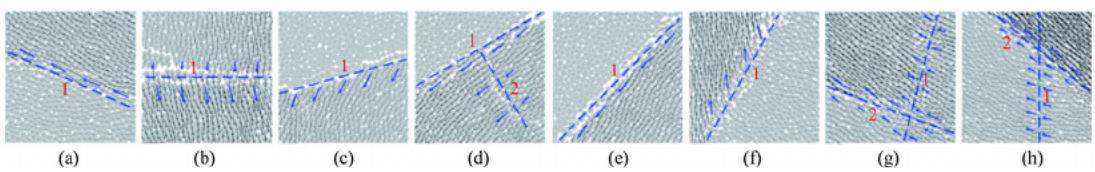

Fig. 9. Zoom-in views of some macroscopic cracks shown in Fig. 8.

The ultimate failure patterns of specimens under the impact velocity of 4 and 12 m/s are presented in Fig. 10. It can be found that failure mode of each specimen was similar to its counterpart under different impact velocities. Specimens with angle of 30° and 45° were damaged only marginally compared to the others in all loading conditions. With the impact velocity increasing from 4 to 12 m/s, specimens were crushed to more and more fragments fractured by increasing cracks.

3.2. Mechanical properties

Fig. 11 presents stress-time curves and the dynamic strength of numerical specimens. When impact velocity was 4 m/s, post-peak strain of specimens except those with bedding angle of 30° and 45° decreased to a certain extent. The elastic rebound indicates those specimens were not completely damaged under such a lower impact velocity. When impact velocity increased to 8 and 12 m/s, residual strain for all specimens was greater than their peak strain. Stress dropped steeply in other specimens during the post-peak stage while changes were much flatter in specimen with bedding angle of 30° and 45°, which corresponded to the specimen failure intensity mentioned above.

It can be observed from Fig. 11d that the dynamic strength fluctuated in the range from 16.4 to 22.6 MPa under the impact velocity of 4 m/s, from 21.6 to 28.1 MPa under 8 m/s and from 25.0 to 33.8 MPa under 12 m/s, respectively. Though the dynamic strength increased with impact velocity, its changing tendencies with bedding angle at different impact velocity levels were similar. The peak stress dropped sharply to the bottom when the bedding angle θ increased from 15° to 30° and remained stable with θ increasing to 45°, then rose again. In all conditions, the intact specimen has the maximum dynamic strength, followed by specimens with horizontal and vertical bedding planes, while the dynamic strength of the specimen with θ of 30° stood at the lowest level. This suggests that dynamic mechanical properties of specimens are degraded by bedding planes and influenced by bedding angle.

3.3. Elastic strain energy evolution

The evolution tendencies of elastic strain energy in different specimens presented in Fig. 12 are similar to those of stress, which suggests that accumulated energy level relates positively to stress level within a specimen. It is clear that the maximum elastic strain energy of each specimen increased with impact velocity. Take the specimen with $\theta = 0°$ for example, its maximum strain energy

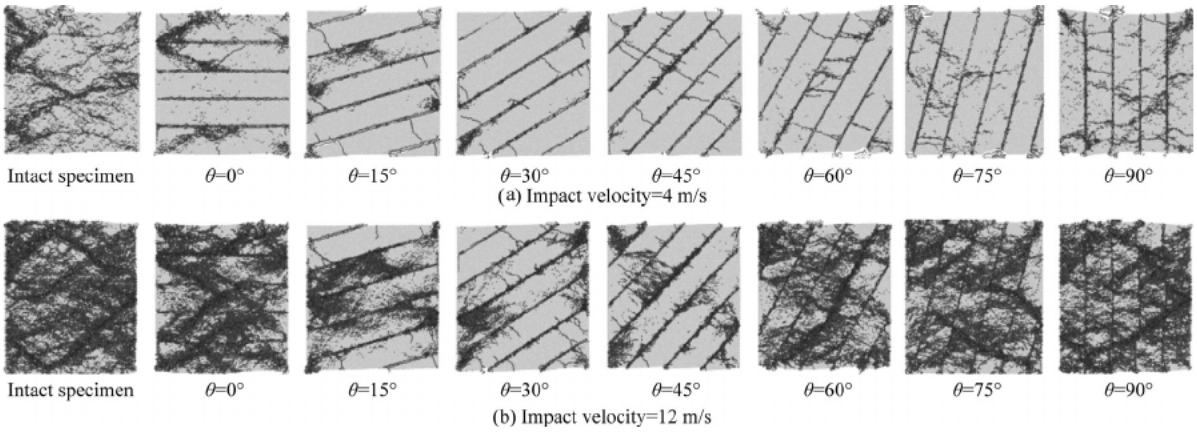

Fig. 10. Ultimate failure mode of different specimens under impact velocity of 4 and 12 m/s.

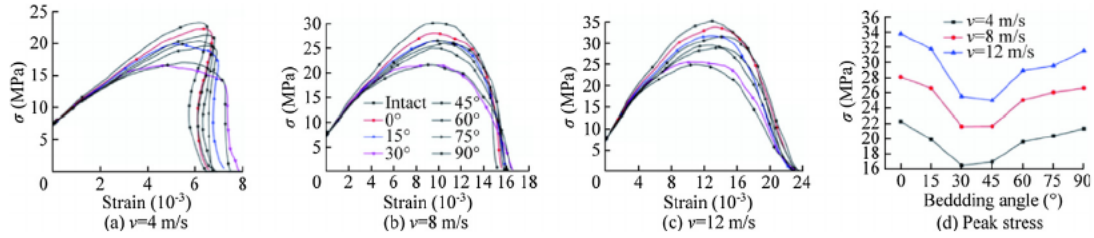

Fig. 11. Stress-time curves and peak stress of different specimens under different impact velocities.

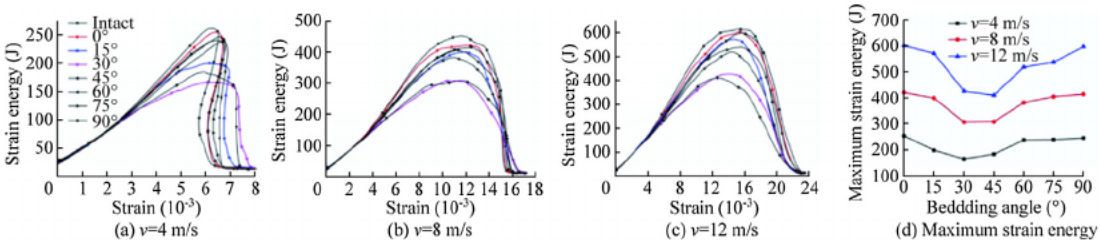

Fig. 12. Elastic strain energy-strain curves and peak elastic strain energy of different specimens under different impact velocities.

increased by 167.7 J when impact velocity increased from 4 to 8 m/s and by 179.9 J when the velocity increased from 8 to 12 m/s, denoting that energy absorbing and releasing are more significate under strong loads. Maximum strain energy also fluctuated more significantly with θ increasing when impact velocity increases. When θ increased from 0° to 30°, the maximum strain energy declined by 88.9, 114.2 and 174.6 J respectively as impact velocity increased, indicating that accumulated energy gets more sensitive to bedding angle under a stronger impact.

4. Discussion

4.1. Bedding influence on mechanical properties

The study suggests that bedding planes degrade both strength and maximum strain energy for specimens. To quantitatively evaluate the influence, strength decay coefficient k_s and energy decay coefficient k_e are introduced and defined as:

$$k_s = 1 - \sigma = \sigma_{intact} \tag{4}$$

$$k_e = 1 - E = E_{intact} \tag{5}$$

where σ_{intact} and E_{intact} are the strength; and maximum strain energy of intact specimen σ and E are the strength and maximum strain energy of specimen containing bedding planes under the same loading condition.

As shown in Fig. 13a, in all tests, bedding planes parallel to the loading direction ($\theta = 0°$) have a minimal impact on specimen strength with the minimum k_s less than 0.07. When bedding planes inclined to 15°, k_s rose up into the range from 0.10 to 0.15. When θ increased to 30° and 45°, bedding planes reached the peak of their influence with k_s fluctuating between 0.27 and 0.29, showing that they reduced strength significantly in this case. Afterwards, the influence began to fade as bedding planes continued to incline to 90°.

As to k_e, similar tendency was observed in Fig. 13b. Bedding planes damaged the ability of specimens to absorb strain energy most significantly with k_s in the range from 0.29 to 0.36 when θ was within the range of 30° to 45°, which reduced released energy to a large extent and was considered to restrain the rock burst propensity.

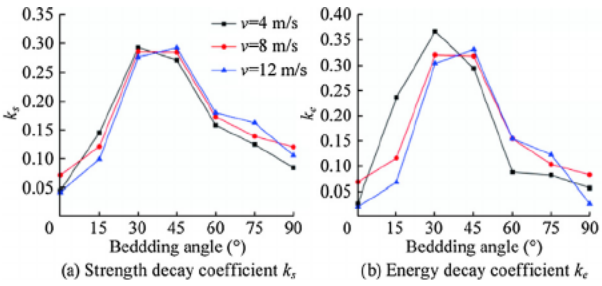

Fig. 13. Strength decay coefficient k_s and energy decay coefficient k_e for different specimens.

Fig. 14 explains the simplified dynamic influence of bedding planes using Hopkinson effect. For specimens whose bedding planes are perpendicular to the dynamic loads (Fig. 14c), when the incident wave (P_i) arrives at the surface of a bedding plane, only part of it would pass through the bedding plane as transmitted wave (P_t), and the other part was reflected as reflected wave (P_r). Each interaction between loads and bedding planes is accompanied by energy dissipation and possible failure. For a specimen containing inclined bedding planes (Fig. 14b), the reflected wave (P_r) can be decomposed into two components perpendicular or parallel to the bedding plane respectively (P_{r1} and P_{r2}). P_{r2} may cause shear failure along the bedding plane while P_{r1} contributes to possible tensile failure perpendicular to the bedding plane. As the tensile and shear strength of bedding planes are much lower, the specimen would be damaged into several parts. Each part would keep intact to a certain extent.

However, for specimens intact or containing horizontal bedding planes (Fig. 14a), there is neither reflected wave nor transmitted wave during the whole process, and elastic strain energy would continually accumulate until the specimen suddenly damages. Change of their elastic strain energy is very sharp, with specimens being crushed to small pieces of fragments by their highly absorbed energy.

4.2. Bedding influence on burst propensity

Elastic strain energy will be released once instability occurs, then convert into kinetic energy and form more micro cracks and crack planes. Therefore, there is a positive correlation between elastic strain energy and burst propensity. In this study, elastic strain energy combined with failure mode was employed to characterize the burst propensity of different specimens. As discussed above, a higher value of maximum elastic strain energy corresponds to a severe failure as happened to the intact specimen or those with θ of 0°, 75° and 90°. Meanwhile, the elastic strain energy in specimens with angle of 30° and 45° is much lower and not likely to induce coal bump. As the maximum strain energy, which is the source of kinematic energy at the post-peak stage, was highest in intact specimen and increased with impact velocity, intact coal is most likely to suffer coal bump especially under strong dynamic loads.

5. Conclusions

Failure behaviour and energy evolution of specimens containing bedding planes in the pre-load SHPB test were investigated in this research using numerical simulation soft PFC2D. Based on the simulation results, the following conclusions can be drawn:

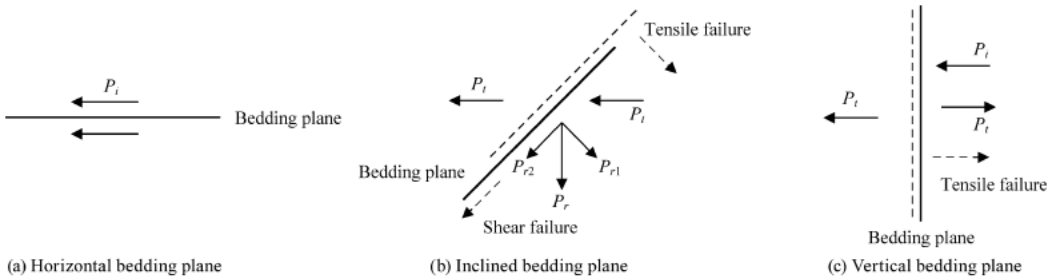

Fig. 14. Interaction between dynamic loads and bedding plane with different bedding angle.

(1) Bedding planes in a coal specimen lead to the degradation of its mechanical properties under coupled static and dynamic loads. This influence is closely associated with angle θ between bedding planes and the loading direction. With θ increasing, specimen strength as well as its maximum strain energy firstly decreases and then increases showing a V-shape trend. When bedding planes are parallel to the loading direction, they have the minimum effect on specimen's dynamic mechanical behavior. Inclined bedding planes cause the most severe degradation of dynamic strength. Besides, this influence is more prominent in SHPB test with a higher impact velocity than in those with a lower impact velocity.

(2) Bedding planes with different θ affect the failure mode of coal specimens to varying degrees. Overall, five failure patterns can be classified for coal specimens containing bedding planes under coupled static and dynamic loads: (a) sliding shear failure along bedding planes; (b) splitting tensile failure along bedding planes; (c) tensile failure through bedding planes; (d) shear failure through bedding planes; and (e) mixed tensile-shear failure.

(3) For specimens containing bedding planes, when dynamic loads are inclined to bedding planes, specimens are most vulnerable to bedding sliding failure, but coal bump and burst are not likely to appear in such coal as their capacity for storing elastic strain energy is limited. With a transient process of huge energy accumulation and release, the burst propensity of specimens whose bedding planes are parallel or perpendicular to dynamic loads is most obvious.

Acknowledgement

The first author thanks the Chinese Scholarship Council (No. 201706370022) for the financial support to the joint Ph.D. programme at the University of Wollongong, Australia.

References

[1] Zhou Z, Li X, Zou Y, Jiang Y, Li G. Dynamic Brazilian tests of granite under coupled static and dynamic loads. Rock Mech Rock Eng 2014;47(2):495–505.
[2] Huang R, Wang X. Analysis of dynamic disturbance on rock burst. Bull Eng Geol Environ 1999;57(3):281–4.
[3] Kaiser PK, Cai M. Design of rock support system under rockburst condition. J Rock Mech Geotech Eng 2012;4(3):215–27.
[4] Xu Y, Dai F. Dynamic response and failure mechanism of brittle rocks under combined compression-shear loading experiments. Rock Mech Rock Eng 2018;51(3):747–64.
[5] Zhang QB, Zhao J. A review of dynamic experimental techniques and mechanical behaviour of rock materials. Rock Mech Rock Eng 2014;47(4):1411–78.
[6] Zou C, Wong LNY. Experimental studies on cracking processes and failure in marble under dynamic loading. Eng Geol 2014;173:19–31.
[7] Li M, Mao X, Lu A, Tao T, Zhang GH, Zhang LY, et al. Effect of specimen size on energy dissipation characteristics of red sandstone under high strain rate. Int J Min Sci Technol 2014;24(2):151–6.
[8] Feng J, Wang E, Chen X, Ding H. Energy dissipation rate: an indicator of coal deformation and failure under static and dynamic compressive loads. Int J Min Sci Technol 2017.
[9] Li X, Zou Y, Zhou Z. Numerical simulation of the rock SHPB test with a special shape striker based on the discrete element method. Rock Mech Rock Eng 2014;47(5):1693–709.
[10] Imani M, Nejati HR, Goshtasbi K. Dynamic response and failure mechanism of Brazilian disk specimens at high strain rate. Soil Dyn Earthquake Eng 2017;100:261–9.
[11] Li X, Zhou Z, Lok T, Hong L, Yin T. Innovative testing technique of rock subjected to coupled static and dynamic loads. Int J Rock Mech Min Sci 2008;45(5):739–48.
[12] Tao M, Ma A, Cao W, Li X, Gong F. Dynamic response of pre-stressed rock with a circular cavity subject to transient loading. Int J Rock Mech Min Sci 2017;99:1–8.
[13] Yang Z, Chen J, Huang T. Effect of joint sets on the strength and deformation of rock mass models. Int J Rock Mech Min Sci 1998;35(1):75–84.
[14] Zhang X, Yang J, Liu B. Experimental study on anisotropic strength properties of sandstone. In: ISRM international symposium on rock mechanics-SINOROCK 2009. International Society for Rock Mechanics; 2009.
[15] Tavallali A, Vervoort A. Failure of layered sandstone under Brazilian test conditions: effect of micro-scale parameters on macro-scale behaviour. Rock Mech Rock Eng 2010;43(5):641–53.
[16] Rongkun P, Dong F, Minggao Y, Lei C. Directivity effect of unloading bedding coal induced fracture evolution and its application. Int J Min Sci Technol 2017;27(5):825–9.
[17] Liu K, Liu Q, Zhu Y, Liu B. Experimental study of coal considering directivity effect of bedding plane under Brazilian splitting and uniaxial compression. Chin J Rock Mech Eng 2013;32(2):308–16.
[18] Baud P, Louis L, David C, Rawling GC, Wong T. Effects of bedding and foliation on mechanical anisotropy, damage evolution and failure mode. Geol Soc Spec Publ 2005;245(1):223–49.
[19] Wasantha P, Ranjith P, Shao S. Energy monitoring and analysis during deformation of bedded-sandstone: use of acoustic emission. Ultrasonics 2014;54(1):217–26.
[20] Amadei B. Strength of a regularly jointed rock mass under biaxial and axisymmetric loading conditions. Int J Rock Mech Min Geo Abs 1988;25(1):3–13.
[21] Zhao Y, Zhao G-F, Jiang Y, Elsworth D, Huang Y. Effects of bedding on the dynamic indirect tensile strength of coal: laboratory experiments and numerical simulation. Int J Coal Geol 2014;132:81–93.
[22] Liu X, Dai F, Zhang R, Liu J. Static and dynamic uniaxial compression tests on coal rock considering the bedding directivity. Environ Earth Sci 2015;73(10):5933–49.
[23] Xie H, Li L, Peng R, Ju Y. Energy analysis and criteria for structural failure of rocks. J Rock Mech Geotech Eng 2009;1(1):11–20.
[24] Wang J, Park H. Comprehensive prediction of rockburst based on analysis of strain energy in rocks. Tunn Undergr Sp Tech 2001;16(1):49–57.
[25] Yang S, Huang Y, Jing H, Liu X. Discrete element modeling on fracture coalescence behavior of red sandstone containing two unparallel fissures under uniaxial compression. Eng Geol 2014;178:28–48.
[26] Zhou Z, Tan L, Cao W, Zhou Z, Cai X. Fracture evolution and failure behaviour of marble specimens containing rectangular cavities under uniaxial loading. Eng Fract Mech 2017;184:183–201.
[27] Zhao Y, Liu S, Jiang Y, Wang K, Huang Y. Dynamic tensile strength of coal under dry and saturated conditions. Rock Mech Rock Eng 2016;49(5):1709–20.
[28] Hong L, Zhou ZL, Yin TB, Liao GY, Ye ZY. Energy consumption in rock fragmentation at intermediate strain rate. J Central South Univ Technol 2009;16(4):677–82.
[29] Ravichandran G, Subhash G. Critical appraisal of limiting strain rates for compression testing of ceramics in a split Hopkinson pressure bar. J Am Ceram Soc 1994;77(1):263–7.
[30] Zhang X, Wong LNY. Displacement field analysis for cracking processes in bonded-particle model. Bull Eng Geol Environ 2014;73(1):13–21.